applied sciences

MDPI

Article

Effects of Vehicle Speed on Vehicle-Induced Dynamic Behaviors of a Concrete Bridge with Smooth and Rough Road Surfaces

Li Dai [1], Mi-Da Cui [2], Ze-Wen Zhu [1,3], Yi Li [2], Jiang-Rui Qiu [2] and Xiao-Xiang Cheng [2,*]

1 Jiangxi Institute of Transportation Research Co., Ltd., Nanchang 330200, China
2 School of Civil Engineering, Southeast University, Nanjing 211189, China
3 Research and Development Center on Technologies and Equipment of Long-Span Bridge Construction, Ministry of Transport, Nanchang 330200, China
* Correspondence: cxx_njut@hotmail.com

Abstract: According to a previous study, a concrete bridge bearing vehicles traveling at lower speeds suffers from more severe apparent damage compared to one bearing vehicles traveling at higher speeds. The authors of the study subjectively inferred that the observed phenomenon is due to different vehicle load-holding durations for different vehicle speeds. However, this interpretation is not true for bridges with a smooth road surface. Based on an engineering case study of Renyihe Bridge (a concrete rigid-frame continuous highway bridge with spans of 80 m + 4 × 145 m + 80 m), this article reveals via numerical simulations that with the increase in road surface roughness, the resonant responses of the bridge are significantly amplified for cases of low vehicle speed, which can well explain the phenomenon observed by the aforementioned study. Field experiments undertaken on Renyihe Bridge further reveal the related mechanism. These experiments reveal that the frequency of the vehicle excitation for a bridge with sufficient road surface roughness might be closer to the low-order natural frequencies of a bridge with a decrease in vehicle speed. Therefore, the resonant responses are supposed to be more significantly amplified in cases of low vehicle speed after an increase in road surface roughness.

Keywords: concrete bridge; dynamic behavior; vehicle speed; road surface roughness

Citation: Dai, L.; Cui, M.-D.; Zhu, Z.-W.; Li, Y.; Qiu, J.-R.; Cheng, X.-X. Effects of Vehicle Speed on Vehicle-Induced Dynamic Behaviors of a Concrete Bridge with Smooth and Rough Road Surfaces. *Appl. Sci.* **2023**, *13*, 9460. https://doi.org/10.3390/app13169460

Academic Editor: Angelo Luongo

Received: 20 July 2023
Revised: 3 August 2023
Accepted: 9 August 2023
Published: 21 August 2023

1. Introduction

In-service highway concrete bridges bear vehicle loads every day, with strong dynamic coupling effects [1–3]. In order to shoulder the heavy traffic burden, multiple lanes are usually set along the transverse direction on the deck of a highway bridge. According to Chinese national traffic regulations, the speeds of vehicles running on different lanes are limited to different ranges. In China, the vehicle speed should increase if the vehicle changes its transverse position from a right lane to a left lane. For example, it is stipulated by Chinese regulations that the speed ranges are 60–90 km/h, 90–110 km/h, and 110–120 km/h for the right-most lane, the middle lane and the left-most lane, respectively, on a three-lane highway bridge. Based on years of practical experience, it has been found that the beam bodies bearing lanes with different speed ranges usually suffer from varying degrees of damage. According to Ref. [4], it was observed on a 4539 m super-large continuous concrete girder bridge put into service for around 20 years that a beam supporting vehicles running at lower speeds suffers from more severe apparent problems compared with a bridge bearing vehicles traveling at higher speeds. To reveal the mechanisms behind this scientific issue, in-depth studies were undertaken by Ref. [4] following an on-site survey. By using a numerical platform to simulate the scenarios of a vehicle running through a section of the bridge at different speeds and via comparisons between the structural responses calculated for different vehicle speeds, it was observed that the maximum dynamic responses (vehicle-induced deflection and internal force) are roughly the same between different cases. However, the vehicle load-holding duration is longer for low vehicle speeds than for high vehicle speeds. The authors of Ref. [4] concluded that the beams bearing vehicles of lower speeds are therefore of poorer quality.

Regarding this problem, the present article offers a viewpoint different from Ref. [4]. According to the data reported in Ref. [4], the vehicle-induced maximum stress calculated is much lower than the material strength of the concrete, and the structure is proven to be in safe elastic states throughout the loading process. For a bridge constructed using concrete to ensure that the stress is no greater than the material strength, it is widely acknowledged that the load-holding duration does not have a significant influence on the degree of damage on the structure, as the concrete material is not prone to non-strength failures (e.g., fatigue failure). Therefore, the contention presented in Ref. [4] that the observed phenomenon is due to the vehicle load-holding duration is unreasonable. On the other hand, a drawback is also noted for the numerical simulations presented in Ref. [4]; i.e., the road surface roughness is not taken into account by the performed analyses. According to Refs. [5–8], the road surface roughness has noticeable effects on the vehicle–bridge dynamic interaction. As almost all actual bridges are associated with varying degrees of road surface roughness, we have reason to suspect that the different degrees of dynamic amplification due to road surface roughness could explain why beams bearing vehicle loads running at different speeds are subjected to dynamic action of different intensities. In the past, a lot of effort has been devoted to exploring related matters of engineering, such as the vibration analysis of multi-span beams subjected to moving loads and masses [9–12] and the dynamic response of bridge-like structures subjected to moving loads at a small scale [13–16]. For example, Zhu and Law [9] developed a method based on the modal superposition and regularization technique to identify moving loads on an elastically supported multi-span continuous bridge deck. Kiani et al. [10] studied the dynamic response of multi-span visco-elastic thin beams subjected to a moving mass by an efficient numerical method. Johansson et al. [11] devised a closed-form solution for evaluating the dynamical behavior of a general multi-span Bernoulli–Euler beam. Szyłko-Bigus et al. [12] considered the dynamic behavior of a Rayleigh multi-span uniform continuous beam system that is traversed by a constant moving force or a uniformly distributed load, and the problem was solved using an analogue of the static force method. Kiani and Roshan [13] studied transverse vibrations of doubly parallel nanotubes acted upon by doubly lagged-moving nanoparticles accounting for non-locality. Yu et al. [14] studied the non-local transverse vibrations of vertically aligned single-layered membranes from single-walled carbon nanotubes for transporting nanoparticles. Abdelrahman et al. [15] developed a nonclassical size-dependent model to study and analyze the dynamic behavior of the perforated Reddy nanobeam under moving load including the length scale and the microstructure effects. Hosseini et al. [16] investigated the dynamic response of a functionally graded nanobeam using a moving load in a thermal environment. It is noted that all of the above-mentioned studies employed analytical techniques to deal with the scientific issues. Although it is widely acknowledged that the analytical results obtained via mathematical models are of high theoretical significance, studies using other approaches of higher fidelity and reliability (e.g., the numerical simulation and the physical test) should also be attempted when possible.

Taking the engineering case study of Renyihe Bridge, a concrete rigid-frame continuous highway bridge with spans of 80 m + 4 $\times$ 145 m + 80 m, the present article uses in-depth numerical simulations and reliable field physical tests to validate the above-mentioned scientific notion. After an extensive review, it is found that existing studies separately considered the effects of road surface roughness [5–8] and the effects of vehicle speed [9,13–15] on the vehicle–bridge coupling dynamics. However, no study has well revealed the interactions between vehicle speed and road surface roughness in the context of vehicle–bridge coupling dynamics, which is proven to be non-negligible. This scientific gap is filled in this article, which justifies the main contribution of the present work. In addition to the theoretical importance of the present work, its practical significance for concrete bridge maintenance and monitoring is also immeasurable.

2. Engineering Background and Numerical Model

Located in Shanxi Province, China, Renyihe Bridge is a concrete rigid-frame continuous highway bridge with the spans 80 m + 4 × 145 m + 80 m (Figure 1). As shown in Figure 1, the superstructure is a single-cell single-box concrete continuous girder with variable cross-sections. The prestresses are applied to the girder in longitudinal and vertical directions. The bridge was built in 2003 and has been in service since then.

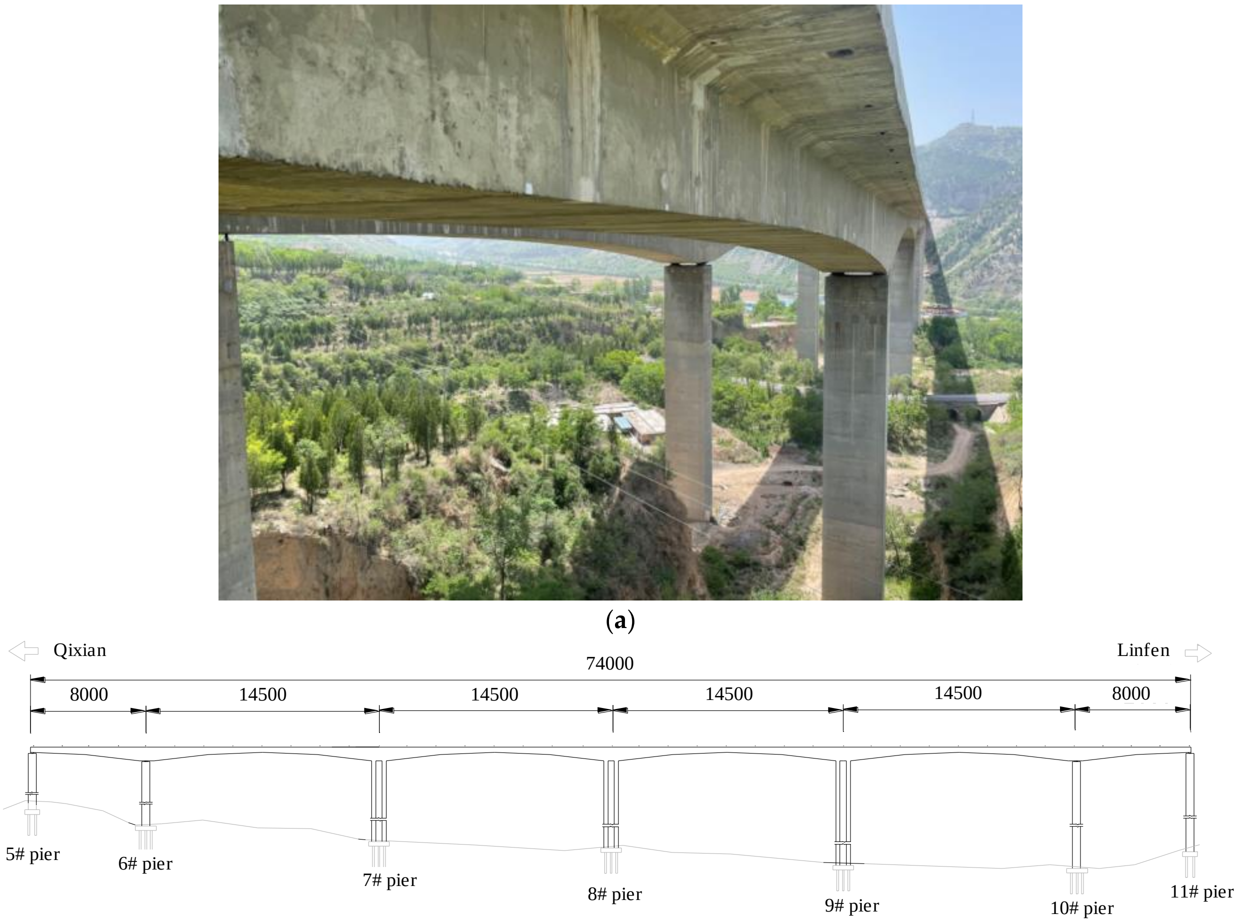

(**a**)

(**b**)

Figure 1. Side view and elevation sketch of Renyihe Bridge. (**a**) Actual side view. (**b**) Elevation sketch (unit: cm).

The finite-element (FE) model of Renyihe Bridge was established on the MIDAS platform (v6.71) using 241 beam elements with 248 nodes with the help of the modeling assistant module provided by the platform (Figure 2). The boundary conditions were assumed to be fixed. The axial stiffness of piers depends on the length of the piers and the tensile/compressive stiffness of the piers. The shorter the length of the piers and the greater the tensile/compressive stiffness of the piers, the higher the axial stiffness of the piers. For the case of Renyihe Bridge, although the length of the piers is comparatively long, the tensile/compressive stiffness of the piers is sufficiently large. Therefore, the axial stiffness of the piers of Renyihe Bridge is still very large, and they can be simply considered rigid. We admit that the simplified beam FE models cannot satisfactorily simulate all the geometric details of the structures and therefore inevitably contain model structure errors. According to our experiences, these errors can hardly be completely eliminated through traditional parameter identification. However, MIDAS is a specialized FE platform designed for bridge engineering, and the beam elements provided by the MIDAS platform are different from those provided by other general FE software (e.g., ANSYS), being able to accurately reflect the realistic sectional properties of the structure. Therefore, the inherent uncertainties associated with the beam model established are greatly reduced on the MIDAS platform. On account of the reduced modeling workload and for the sake of computing efficiency, we finally chose to use the beam model established on the MIDAS platform. The numerical simulation procedure, in order, consisted of basic information (the elevation geometry, the material properties, the division of the structure for construction, and the construction duration) input, cross-section geometry input, and steel strand information input. The geometry of the structure was modeled in detail in accordance with Figure 1b, and the concrete material models adopted were those of uniaxial compression and the tension linear elastic constitutive relation. To take into account the influences of steel strand pre-stressing, the shrinkage and the creep of the concrete, and other effects during the construction stages on the mechanical state of the constructed structure, the model of Renyihe Bridge was established progressively, reflecting each constructional state in temporal order, including the concrete pouring of the piers, the concrete pouring of the 0 blocks above the piers, carriage traveling, the concrete pouring and steel strand tensioning for each block, the closure of the T-shaped structures, and the structural system transformation. Therefore, the simulation process accurately considered the cumulative influences of the multiple constructional effects.

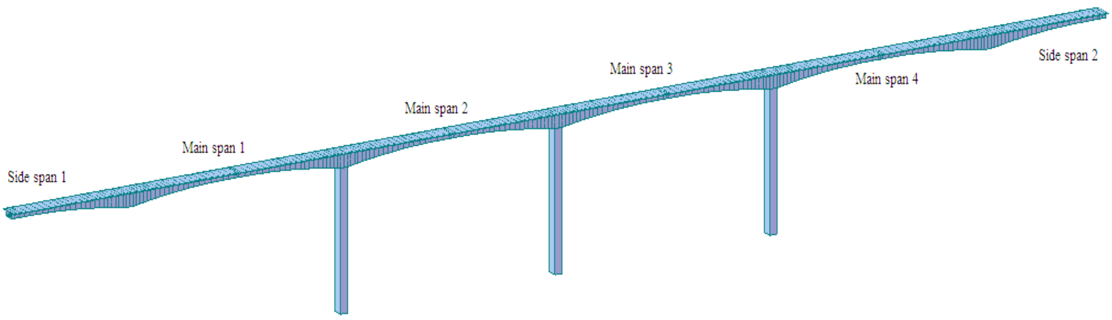

Figure 2. FE model of Renyihe Bridge established on MIDAS platform.

After the FE model of Renyihe Bridge was established, an initial in-plane modal analysis was performed. The results are shown in Table 1 and Figure 3. As can be seen in Table 1, the 1st~18th order natural frequencies calculated using the initial FE model of Renyihe Bridge are distributed uniformly in the frequency interval 0.7–7 Hz, and most of them are greater than 1 Hz, indicating that the vehicle excitations with the energies roughly in the range 2.85–11.8 Hz [17] usually cannot excite the structure's low-order (1st~9th order) resonances. According to Figure 3, all mode shapes calculated for Renyihe Bridge are the girder's vertical bendings, symmetric or antisymmetric. For some modes, the dynamics of the girder and the piers are strongly coupled (Figure 3c,f); for others, they are not coupled.

Table 1. Low-order natural frequencies calculated using the initial FE model.

Mode No.	Calculated Natural Frequency (Hz)	Mode No.	Calculated Natural Frequency (Hz)	Mode No.	Calculated Natural Frequency (Hz)
1	0.73	2	0.79	3	0.96
4	1.19	5	1.52	6	1.68
7	2.02	8	2.43	9	2.68
10	2.86	11	3.99	12	4.21
13	4.49	14	4.83	15	5.71
16	5.75	17	6.56	18	6.90

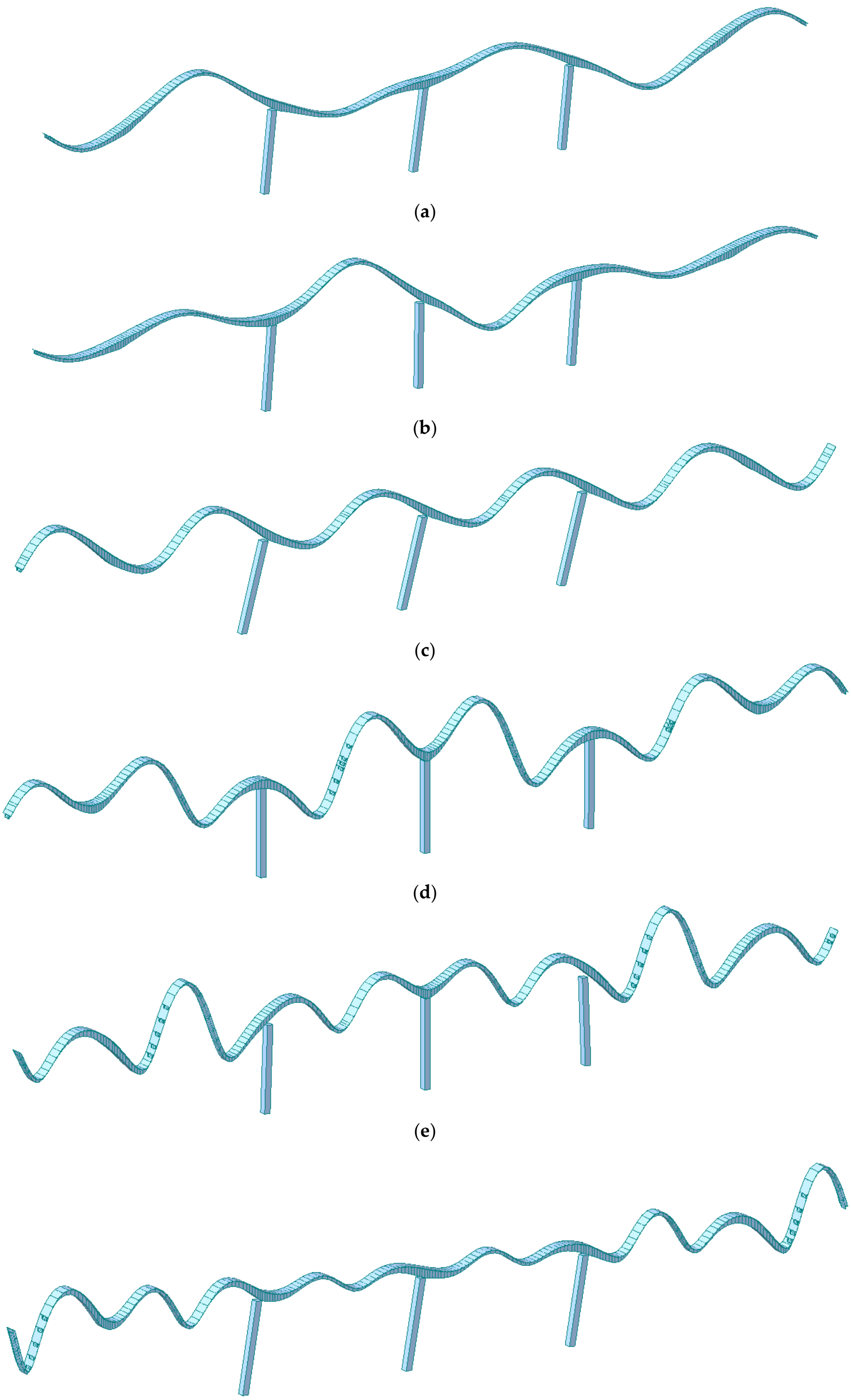

Figure 3. Low-order mode shapes calculated using the FE model: (**a**) 1st mode (0.73 Hz), (**b**) 3rd mode (0.96 Hz), (**c**) 5th mode (1.52 Hz), (**d**) 10th mode (2.86 Hz), (**e**) 12th mode (4.21 Hz), (**f**) 15th mode (5.71 Hz).

3. Simulation of Vehicle-Passing Scenarios

On the MIDAS platform, we attempted to numerically simulate vehicle passing scenarios using the established FE model of Renyihe Bridge. Nine cases were set for the numerical simulations assuming a 30-ton vehicle running through the bridge at three vehicle speeds (20 km/h, 50 km/h, 90 km/h) considering three road surface roughness levels (smooth, slightly rough, severely rough). The reason we simulated three road surface roughness levels is that the road surface is smooth when the bridge is newly built, but the road surface roughness will increase over the years based on the basic rules of physics. With the detailed parameters listed in Table 2, numerical simulations of different vehicle passing cases were undertaken using the time-history analysis method. Taking Case 1 as an example, the vehicle load simulation at a certain point on the bridge deck is described in Figure 4. According to Figure 4, the vehicle load is assumed to be a single vertically downward concentrated force moving at the constant speed of 20 km/h (5.56 m/s). Since the vehicle action on a certain point is a transient impact load that disappears immediately in nature, it can be approximated as a triangular load with the maximum value occurring at the midpoint. As shown in Figure 5, the maximum value of the vehicle action at a certain point in the time domain is calculated as the linear superposition of the gravity of the vehicle body and the road-surface-roughness-induced dynamic action [18]. The road-surface-roughness-induced dynamic action can be calculated as the product of the elevation of the position relative to the initial point Δ (=0 for Case 1) and the additive vertical stiffness of the four attempts (400 kN/m). According to Ref. [18], for a vehicle passing a bridge, it can be assumed that its tires keep contacting the road surface throughout the process, and the vehicle's dynamic action on the bridge can therefore be treated as the sum of the damping force and the elastic force induced by the road surface roughness. As it was found via calculations in Ref. [18] that the damping force is negligible compared with the elastic force, the total vehicle's dynamic action on the bridge roughly equals the elastic force induced by the rough surface roughness, which can be calculated using the method mentioned above. Although this vehicle–road coupling model is simple, its rationality has been proven in practical use [19]. The time-history analysis employed the mode superposition method. Since the accumulative modal participation mass of the 1st~50th modes reaches 96.89%, the main characteristics of the vehicle-induced vertical structural dynamic responses can be captured using the 1st~50th modes. As the natural period of the 50th mode is around 0.05 s, the time-step was set to 0.005 s (=0.05 s/10) for the analysis. The total analysis time was set to 150 s, and the damping ratio was 0.05 for all modes. The vertical acceleration time-history calculated at the mid-span of the 2nd main span in Case 1 and the corresponding amplitude spectrum are shown in Figures 6 and 7, respectively. In Figure 6, when the vehicle is close to the measuring point (70 s~85 s), the acceleration response is significantly amplified, which agrees with the basic rules of physics. As shown in Figure 7, a high peak and a low peak can be observed on the amplitude spectrum at around 1.0 Hz and 3.8 Hz, respectively. The high peak clearly is associated with the vehicle-induced structural resonance at the bridge's low-order natural frequency, while the low peak reflects the existence of the forced vehicle excitation at a high-frequency range. The local area under the high peak of the amplitude spectrum and that under the low peak are defined as the resonant response and the background response, respectively, both of which can be calculated via integration.

Following the same principle, Cases 2~9 were simulated with the respective different road surface roughness levels. To simulate different road surface roughness levels, the elevations of the bridge deck Δ were calculated for the slightly rough road surface roughness case and the severely rough road surface roughness case. First, with reference to Ref. [18], the variation ranges of Δ were set for different cases (-0.01 to 0.01 m and -0.03 to 0.03 m for the slightly rough road surface roughness case and the severely rough road surface roughness case, respectively). Second, the white noise sequences were generated within the variation ranges to form the elevations of the bridge deck. The simulated results of different road surface roughness levels are shown in Figure 8 for use. All numerical simulation results so obtained are presented and discussed in Section 4.

Table 2. Parameters for the numerical simulations of a vehicle passing Renyihe Bridge.

Case	Road Surface Roughness Level	Vehicle Speed (km/h)	Vehicle Weight (ton)
1		20	30
2	Smooth (Δ = 0)	50	30
3		90	30
4		20	30
5	Slightly rough ($\Delta \in [-0.01$ m, 0.01 m])	50	30
6		90	30
7		20	30
8	Severely rough ($\Delta \in [-0.03$ m, 0.03 m])	50	30
9		90	30

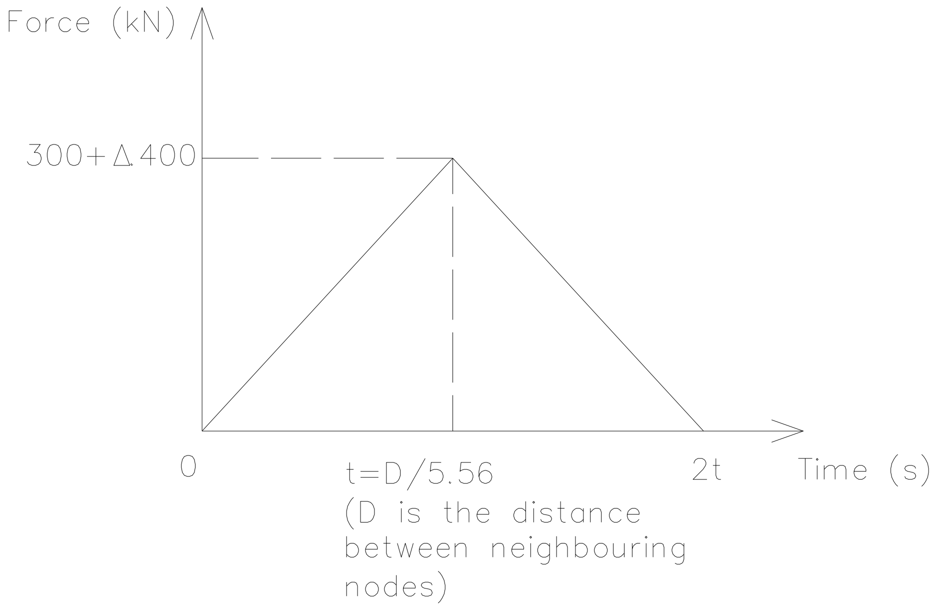

Figure 4. Diagram of vehicle load simulation at a point in Case 1.

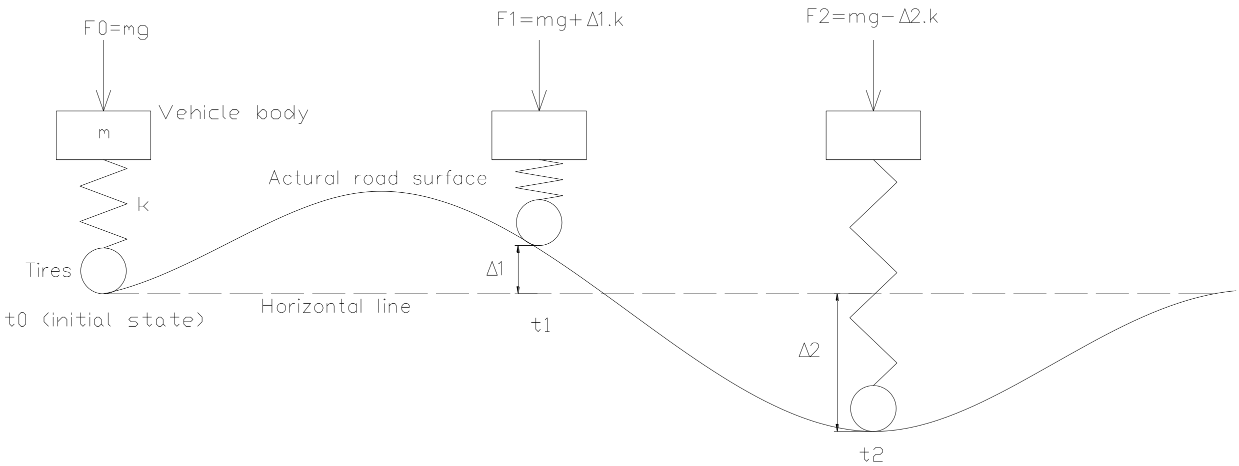

Figure 5. Diagram of the calculation of the maximum vehicle action.

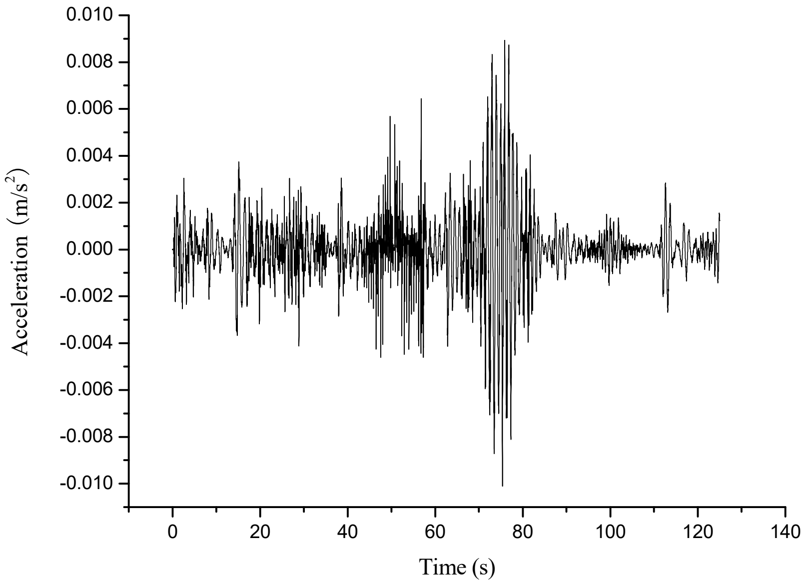

Figure 6. Vertical acceleration time-history calculated at the mid-span of the 2nd main span in Case 1.

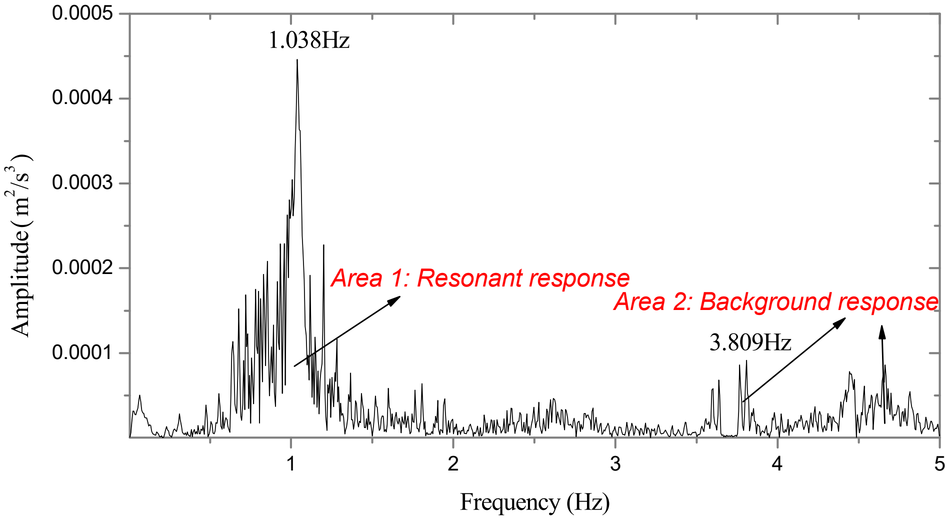

Figure 7. Amplitude spectrum of vertical acceleration calculated at the mid-span of the 2nd main span in Case 1.

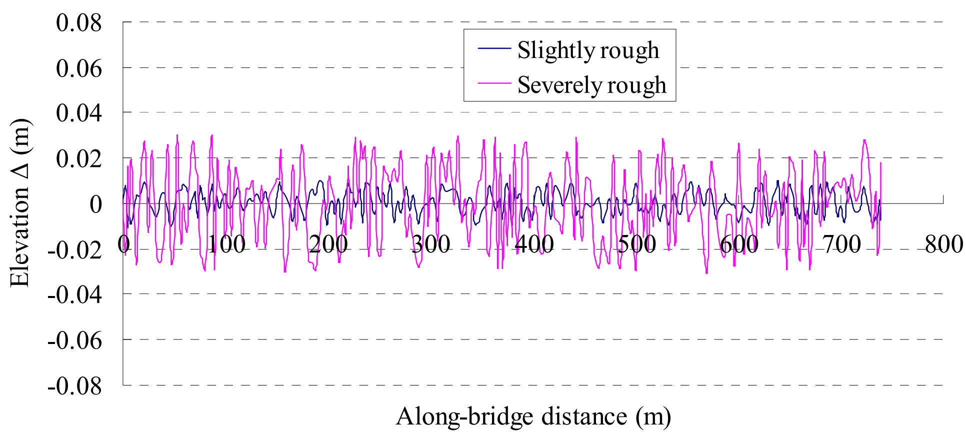

Figure 8. Simulated results of different road surface roughness levels.

4. Numerical Simulation Results

4.1. Smooth Road Surface (Cases 1~3)

With a smooth road surface ($\Delta = 0$), three events of a 30-ton vehicle running through Renyihe Bridge at different speeds were simulated (Cases 1~3). The representative vertical acceleration time-histories for Cases 1~3, which were calculated at the mid-span of the 3rd main span, are compared in Figure 9. As shown, the vehicle-induced structural response of Case 3 is markedly greater than that of Case 2, and the structural response of Case 2 is greater than that of Case 1. These suggest that with the increase in vehicle speed, a greater structural response ought to be induced. To reveal the causation behind this observation, the acceleration time-histories were transformed into amplitude spectra and shown in Figure 10. According to Figure 10, for the amplitude spectra of Cases 1 and 2, the energies are accumulated in the bridge's low-order natural frequencies (the frequency range around 1 Hz), and the background responses are not significant; however, for the spectrum of Case 3, the resonant response in the low-frequency range and the background response in the high-frequency range are comparable, and both of them are significant. These suggest that with increasing vehicle speed, the corresponding increase in structural response should mainly be attributed to the stronger force of vehicle excitation in the high-frequency range. The resonant response is also amplified for the high-vehicle-speed case, but the amplification is not so large as to account for a significant portion of the total response increment.

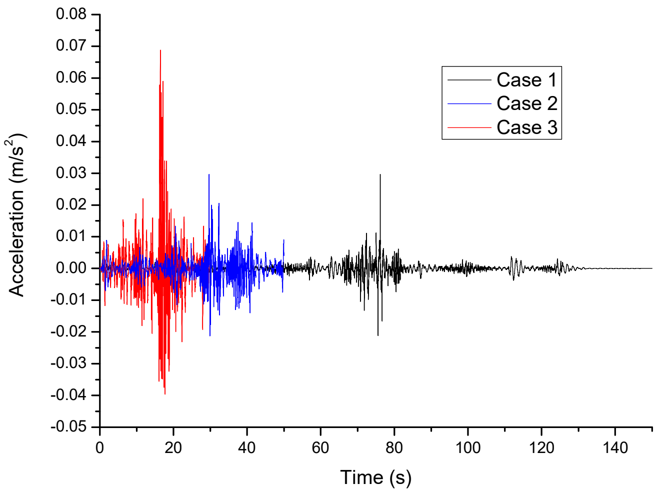

Figure 9. Vertical acceleration time-histories calculated at the mid-span of the 3rd main span in Cases 1~3.

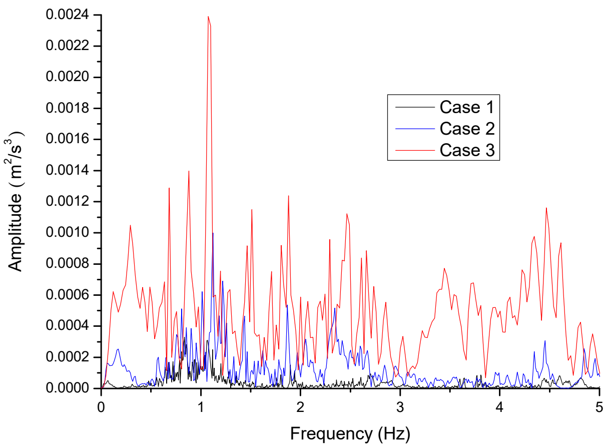

Figure 10. Amplitude spectra of vertical acceleration time-histories calculated at the mid-span of the 3rd main span in Cases 1~3.

The maximum tensile stress distribution on Renyihe Bridge for Case 1 is shown in Figure 11. In Figure 11, the high tensile stresses can be observed at the mid-spans of each span, which agrees with the basic rules of physics. The largest tensile stress for Case 1 is 0.72 MPa, which is much smaller than the tensile strength of C50 concrete (1.89 MPa). Similar situations hold true for Cases 2 and 3, which suggest that without sufficient surface roughness, structural damages are not likely to be induced by the usual vehicles running at various speeds.

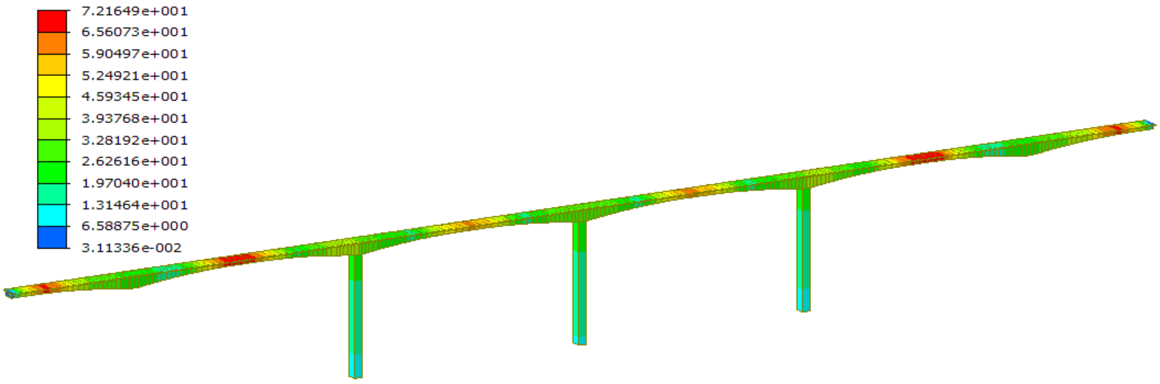

Figure 11. Maximum tensile stress distribution for Case 1 (unit: tonf/m^2).

4.2. Slightly Rough Road Surface (Cases 4~6)

Events of a 30-ton vehicle running through Renyihe Bridge with a slightly rough road surface (Cases 4~6) were also simulated, and the vertical acceleration time-histories calculated at the mid-span of the third main span are shown in Figure 12. Comparing Figure 9 with Figure 12, it can be observed that after the road surface roughness was slightly increased, the vehicle-induced structural responses of different cases did not change at all. After the acceleration time-histories shown in Figure 12 were transformed into amplitude spectra, it can be noted that energy distributions in the frequency domain so obtained for different cases also did not change after the road surface roughness was slightly increased. Due to limited article length, the amplitude spectra and other results are not shown for Cases 4~6 in this portion of study.

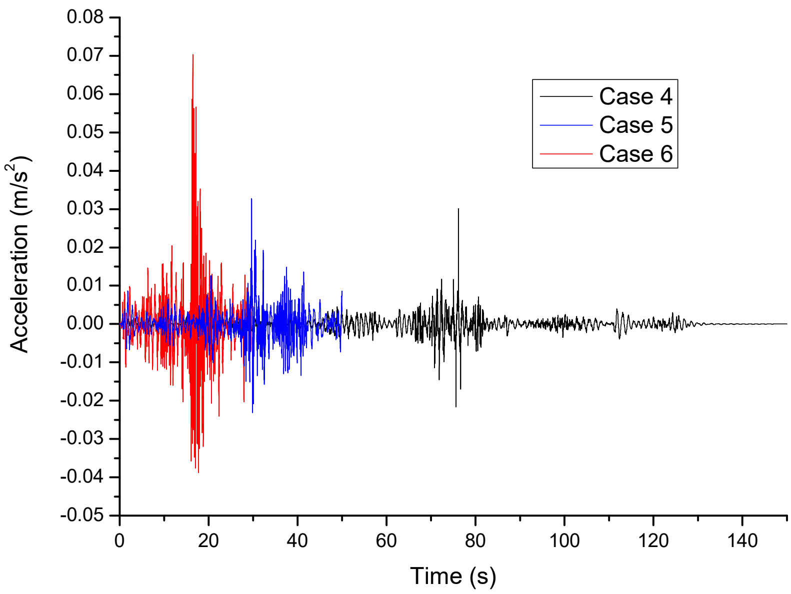

Figure 12. Vertical acceleration time-histories calculated at the mid-span of the 3rd main span in Cases 4~6.

4.3. Severely Rough Road Surface (Cases 7~9)

With respect to the scenarios with the severely rough road surface (Cases 7~9), the calculated results are shown in Figure 13. Comparing the vertical acceleration time-histories calculated at the mid-span of the third main span for Cases 7~8 (Figure 13) with those for Cases 1~3 (Figure 9), it can be observed that with the increase in road surface roughness, the structural responses are significantly amplified for the low-vehicle-speed cases (Cases 7 and 8); however, the structural response for the high-vehicle-speed case (Case 9) is not noticeably amplified after the increase in the road surface roughness, although it is still much greater than those for the low-vehicle-speed cases (Cases 7 and 8). After fast Fourier transformation, the amplitude spectra of vertical acceleration time-histories were obtained (Figure 14). Comparing the amplitude spectra shown in Figures 10 and 14, it can be found that for the low-vehicle-speed cases (Cases 7 and 8), the amplifying effects are mainly reflected in the increased energies in the low-frequency range (at round 1 Hz), indicating that the increased resonant response, rather than background response, accounts for the total response increment. However, why is the resonant response significantly amplified for the low-vehicle-speed cases after the increase in road surface roughness? This important scientific question cannot be well answered via the results obtained in this portion of study.

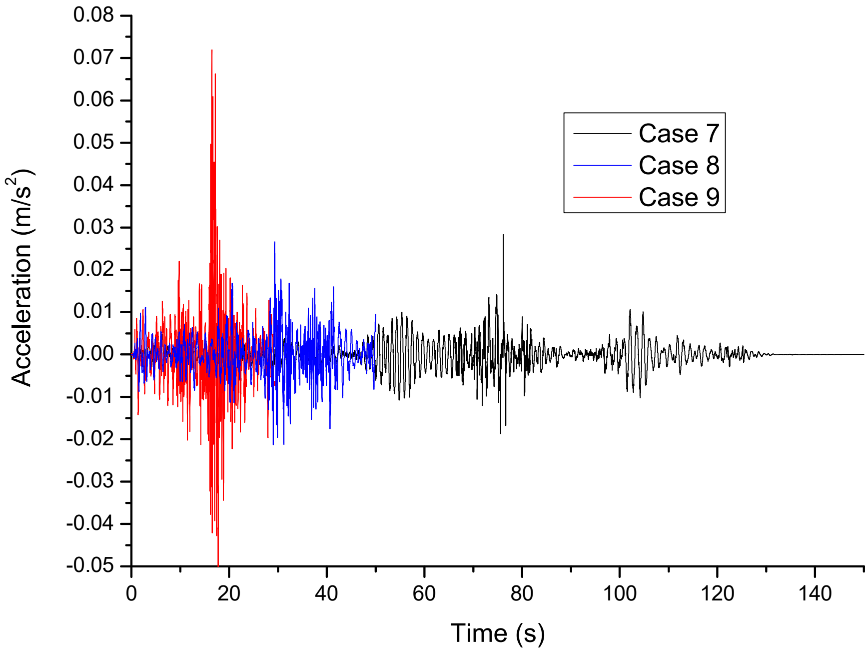

Figure 13. Vertical acceleration time-histories calculated at the mid-span of the 3rd main span in Cases 7~9.

Furthermore, the vehicle-induced maximum tensile stresses on Renyihe Bridge were obtained for Cases 7~9 and compared with those for Cases 1~3 in Figure 15. As shown, the maximum structural responses for most smooth road surface cases (Cases 1 and 2) are at around 0.8 MPa, which is much smaller than the tensile strength of C50 concrete (1.89 MPa); however, those for the severely rough road surface cases (Cases 7 and 8) are all at around 1.4 MPa, which is closer to the tensile strength of C50 concrete. It should be noted that the present numerical simulation simply employs one 30-ton vehicle running through the bridge as the excitation. In actual scenarios, multiple vehicles of weights greater than 30 tons usually simultaneously run on the bridge, therefore possibly causing the vehicle-induced maximum tensile stress on the concrete to be greater than the tensile material strength. This in turn leads to structural damages. The actual bridges generally have the sufficient road surface roughness required to induce structural damages. Only under this condition does the explanation given by Ref. [4] for the observation that a beam supporting vehicles running at lower speeds suffers from more severe apparent damage (i.e., the observed phenomenon is due to different vehicle load holding durations) make sense.

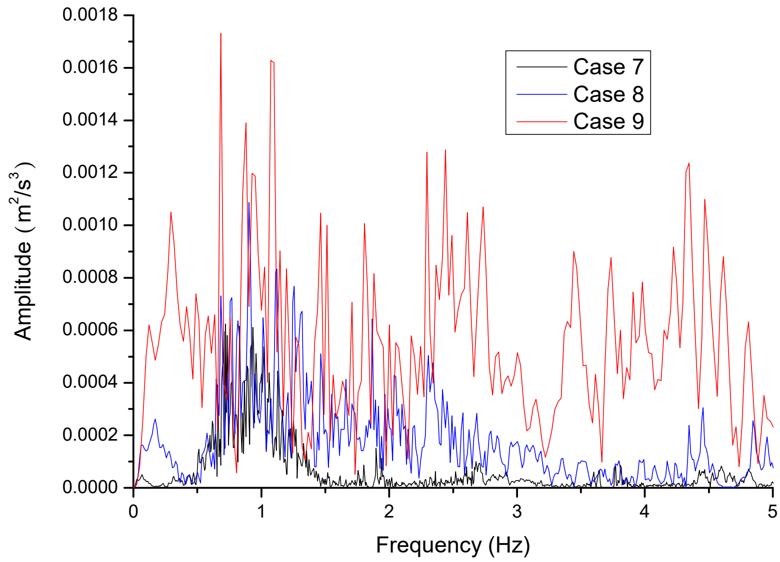

Figure 14. Amplitude spectra of vertical acceleration time-histories calculated at the mid-span of the 3rd main span in Cases 7~9.

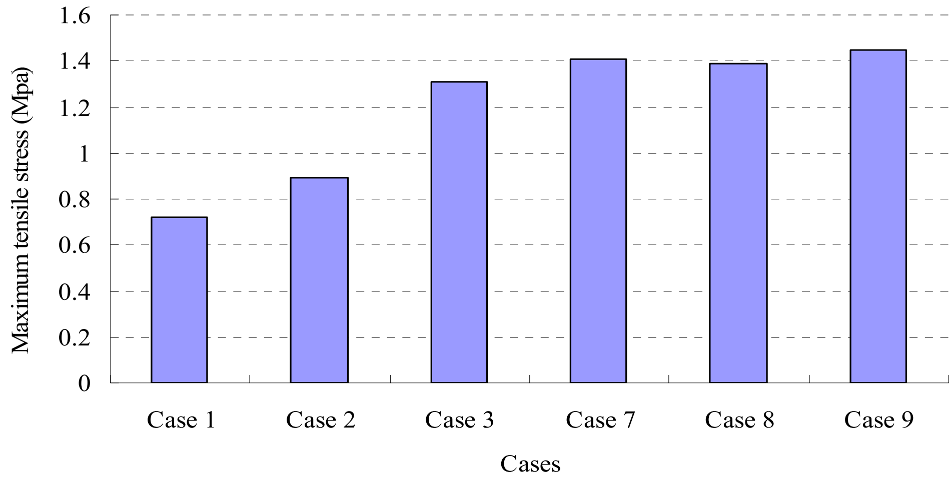

Figure 15. Maximum tensile stresses calculated for different cases.

5. Field Experiments

The field experiments were undertaken in 2021 by the Shanxi Provincial Transportation Construction Engineering Quality Testing Center [20]. Practicing engineers employed two vehicles with weights of around 300 kN, each synchronously running through the bridge at different speeds (Figure 16). Four vehicle speed cases were utilized for the test, i.e., 20 km/h, 30 km/h, 40 km/h, and 50 km/h. According to Ref. [20], the vehicle drivers tried to keep the vehicles moving at the constant speeds. Although the statistics concerning the vehicle speed variations through the entire process were not measured, it was reported that vehicle speed was well controlled, and the effects of the vehicle speed variation on the excitation and the response were reduced to the minimum. For each vehicle speed case, two vertical accelerometers arranged at the mid-span of the third main span (measuring point 1) and the mid-span of the fourth main span (measuring point 2) were utilized to record the vehicle-induced structural velocity responses when the two vehicles ran by them. The structural velocity response samples so obtained (Figures 17 and 18) were then transformed into power spectral densities (PSDs) using fast Fourier transformation (Figures 17 and 18). After that, the first-order natural frequency and the frequency of the forced vehicle excitation were identified from these PSDs via the peak picking method, and the results are listed in Table 3 for reference. According to Table 3, the most fundamental frequencies identified for Renyihe Bridge in different cases are at around 0.77 Hz, which is close to the numerical result presented in Table 1 (0.73 Hz), except for the result measured at the mid-span of the fourth main span in the 20 km/h vehicle speed case (0.82 Hz). The field test results and the numerical data are thereby validated by each other. According to Ref. [17], for bridges excited by passing vehicles, the natural frequencies of the actual system should be independent of excitations and measurements. The good agreements between the fundamental frequencies identified for Renyihe Bridge in different cases by the present study support the contention presented in Ref. [17]. The result measured at the mid-span of fourth main span in the 20 km/h vehicle speed case should also be close to the results measured for other cases. However, on-location physical tests suffer from inherent uncertainties and environmental interferences. Therefore, the field modal test results obtained for different cases might occasionally be different from each other. According to Ref. [19], the natural frequencies of the bridge structure measured are influenced by the velocity and mass weight of the vehicles, as the weight and location of the vehicle become part of some new system. Ref. [19] formulated an approach relying on a dynamic FE model updating to compensate for the deviation in the results of the modal experiment using vehicle excitations due to the adverse effects of running vehicles. In detail, the measurement change in the first modal frequency caused by the running vehicles was captured by on-location modal experiments using both ambient and vehicle excitations, and the equivalent vehicle weight was thereby identified via dynamic FE model updating. Using the updated numerical model, the measurement change in the high-order modal frequency due to the added equivalent vehicle weight was calculated, and the high-order modal frequency measured on location was then compensated for use. However, according to Table 3, the most fundamental frequencies identified for Renyihe Bridge in different cases are at around 0.77 Hz, suggesting that the effects of the velocity and mass weight of the vehicles on the natural frequencies of the bridge are similar for most vehicle speed cases. The focus of the present research is the variation in the frequency difference between the fundamental natural frequency and the frequency of the forced vehicle excitation among different vehicle speed cases, which is not significantly influenced by the velocity and mass weight of the vehicles based on the above. Therefore, the role of the velocity and mass weight of the vehicles does not have to be removed from the plots given in Figures 17 and 18 to arrive at the near-to-exact natural frequencies of the bridge structure for the required study to take place. In addition, in Table 3, the frequencies of the forced vehicle excitation identified for different cases vary in a wide range (2.9–4.0 Hz). This suggests that with sufficient road surface roughness (the variation range of the road surface of the actual Renyihe Bridge is -0.025 to 0.025 m according to Ref. [20]), the nature of the vehicle excitation changes in accordance with the vehicle speed variation. Comparing the 20 km/h vehicle speed case with the 30 km/h vehicle speed case, it can be observed that with the decrease in vehicle speed, the frequency of the vehicle excitation markedly decreases and becomes closer to the low-order natural frequencies of the bridge (the differences between the first-order natural frequencies and the frequencies of the forced vehicle excitation for different cases shown in Figure 19 clearly demonstrate this). Therefore, stronger structural resonances ought to be excited by the passing vehicles when the vehicle speed is reduced. This observation can well answer the question posed in Section 4.3, i.e., why the resonant response is more significantly amplified for a lower vehicle speed case after the road surface roughness is increased. However, by comparing the 20/30 km/h vehicle speed case with the 40/50 km/h vehicle speed case in Figure 19, a different observation is noted; i.e., the frequency difference increases with the decrease in vehicle speed. According to the literature, the energy distribution of the vehicle excitation in the frequency range

(2.85–11.8 Hz) depends on both the road surface roughness and the automobile engine frequency. For the smooth road surface case, the energy distribution totally depends on the automobile engine frequency. According to Figure 10, when the vehicle speed is increased, the energy of the vehicle excitation noticeably shifts to the low-frequency range, suggesting that the automobile engine frequency is decreased. Therefore, for the rough road surface case (the actual Renyihe Bridge), although the nature of the vehicle excitation is influenced due to the effects of road surface roughness when the vehicle speed is decreased, this influence is sometimes not sufficient to bring about the reduction in frequency of the vehicle excitation, as the automobile engine frequency is markedly increased.

Figure 16. Vehicles employed for field experiments.

Table 3. Results of field experiments for different vehicle speed cases.

Vehicle Speed Case	Measuring Point (Vehicle) Location	1st Order Natural Frequency (Hz)	Frequency of the Forced Vehicle Excitation (Hz)	Frequency Difference (Hz)
20 km/h	Measuring point 1	0.777	3.339	2.562
	Measuring point 2	0.82	3.33	2.51
30 km/h	Measuring point 1	0.764	3.756	2.992
	Measuring point 2	0.769	3.95	3.181
40 km/h	Measuring point 1	0.768	3.133	2.365
	Measuring point 2	0.762	3.225	2.463
50 km/h	Measuring point 1	0.767	2.933	2.166
	Measuring point 2	0.768	3.172	2.404

Moreover, strain sensors were arranged at the bottom on the mid-span cross-section of the fourth main span. These sensors were utilized to measure the maximum structural responses of Renyihe Bridge subject to the passing vehicles. The maximum dynamic stresses so obtained in different vehicle speed scenarios are shown in Figure 20. The data presented in Figure 20 agree well with the results presented in Figure 15 for Cases 7~9. The maximum tensile stresses measured on location are comparable to the tensile strength of the material for all vehicle speed cases, suggesting that structural damages could be induced for all cases.

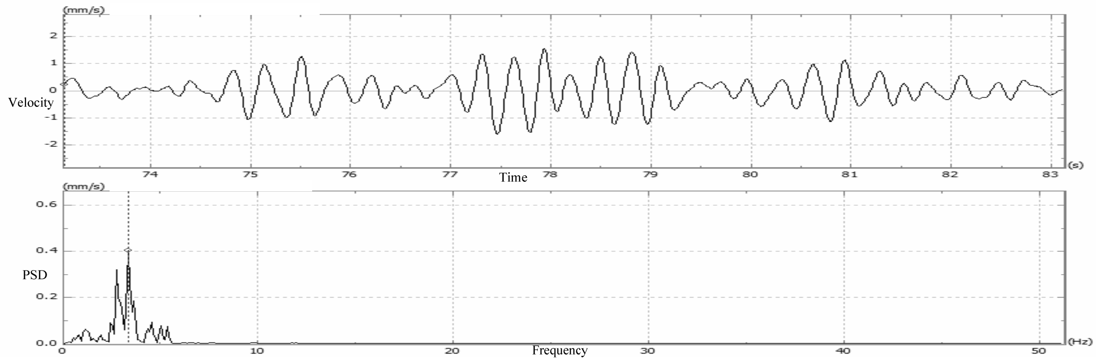

(**a**)

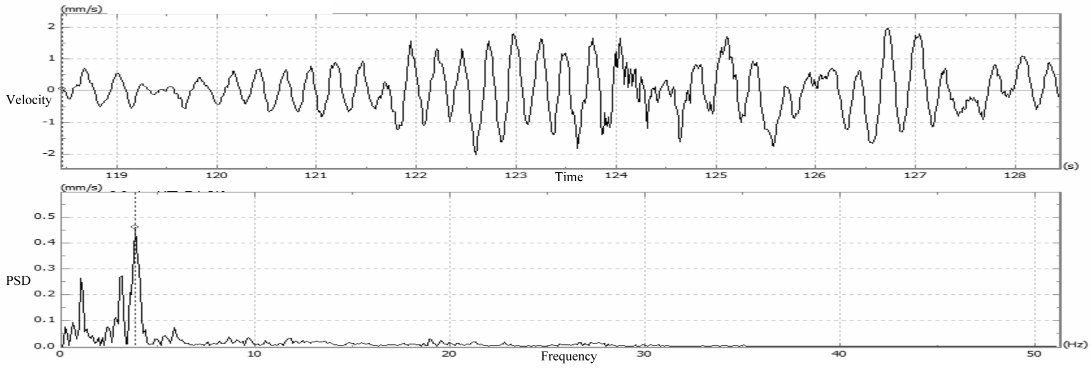

(**b**)

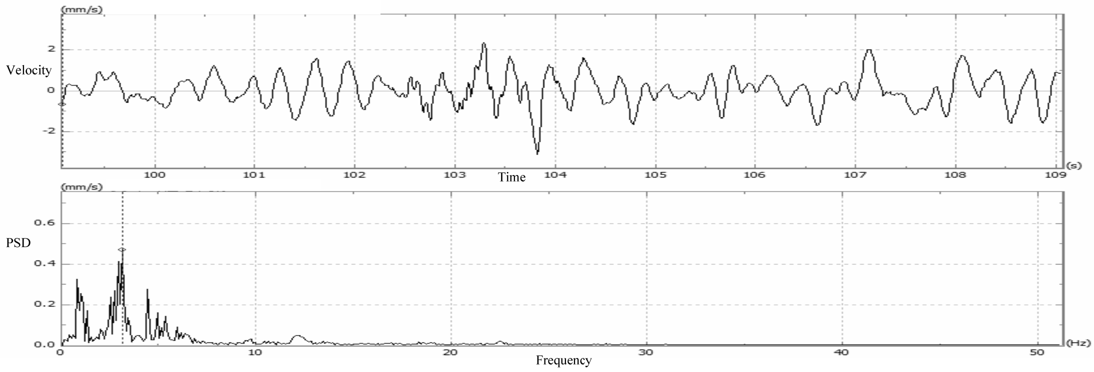

(**c**)

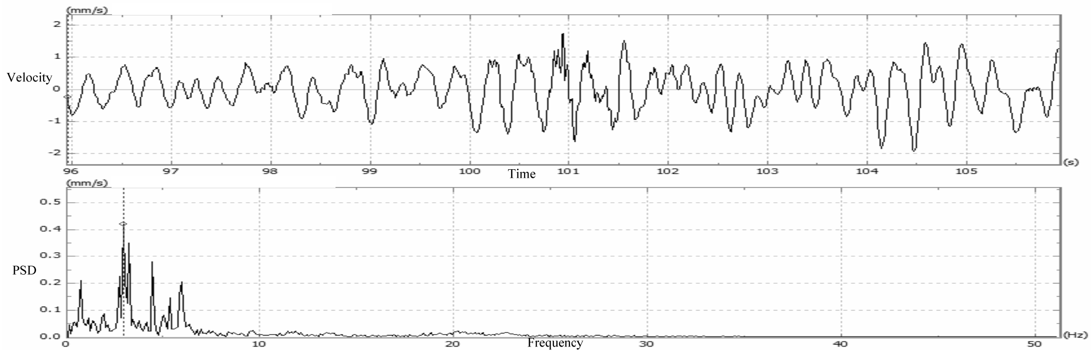

(**d**)

Figure 17. Vertical velocity time-histories and their power spectral densities measured using the accelerometer arranged at measuring point 1: (**a**) 20 km/h vehicle speed, (**b**) 30 km/h vehicle speed, (**c**) 40 km/h vehicle speed, (**d**) 50 km/h vehicle speed.

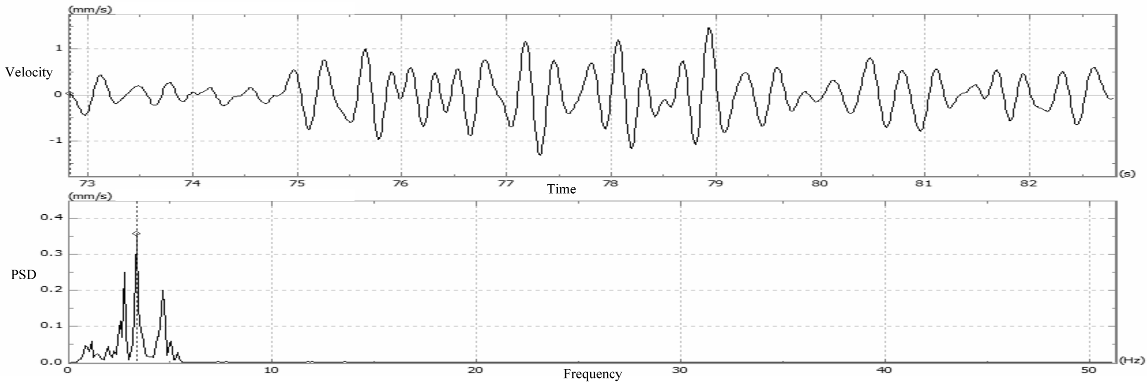

(**a**)

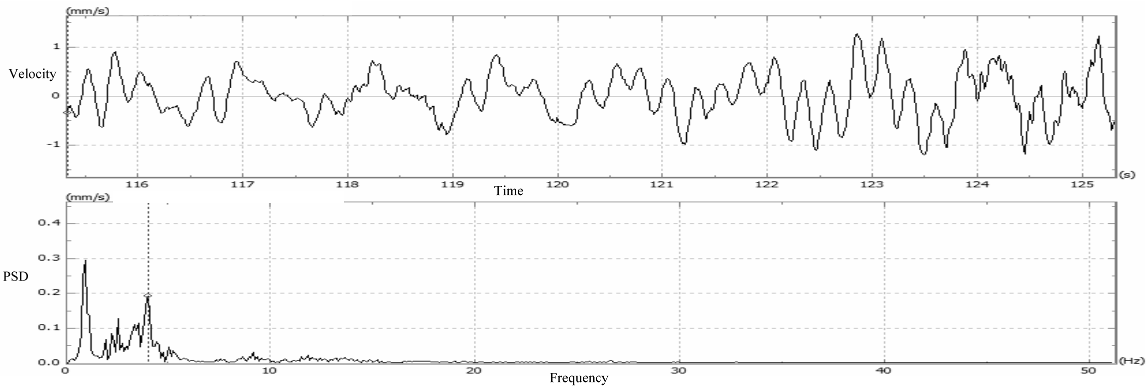

(**b**)

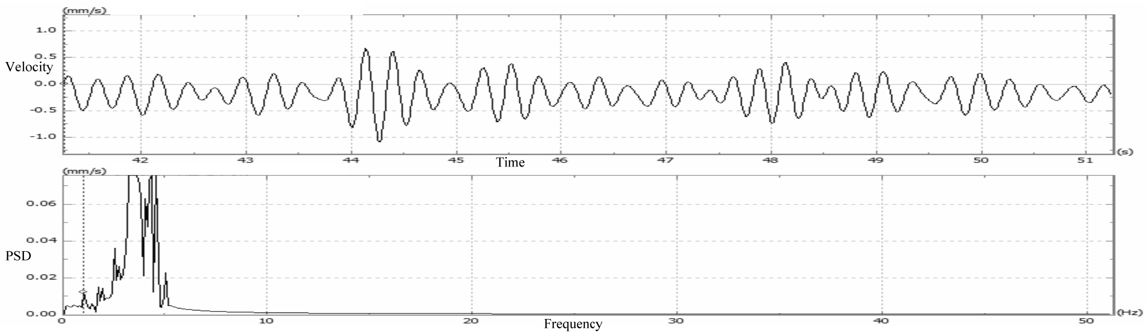

(**c**)

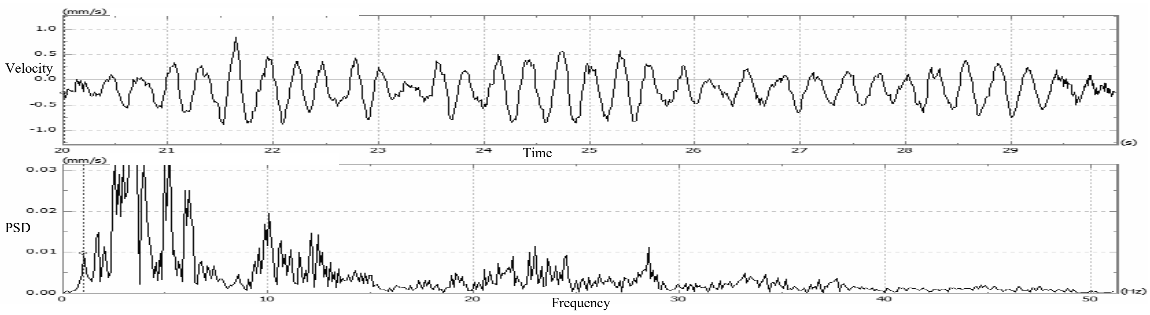

(**d**)

Figure 18. Vertical velocity time-histories and their power spectral densities measured using the accelerometer arranged at measuring point 2: (**a**) 20 km/h vehicle speed, (**b**) 30 km/h vehicle speed, (**c**) 40 km/h vehicle speed, (**d**) 50 km/h vehicle speed.

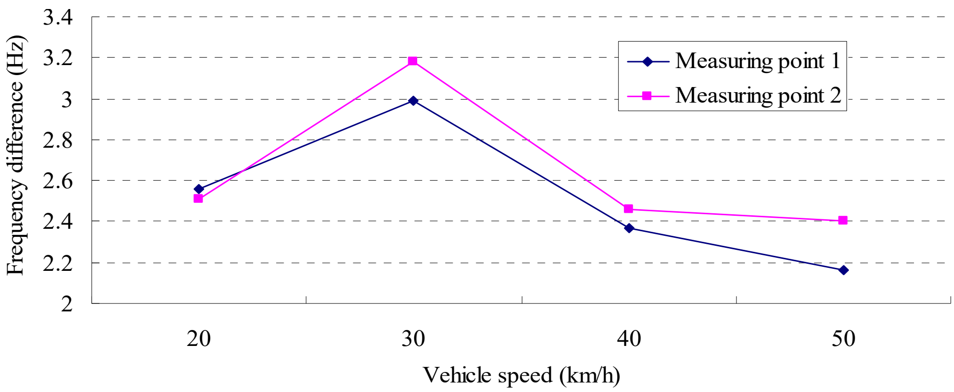

Figure 19. Variation in frequency difference with vehicle speed.

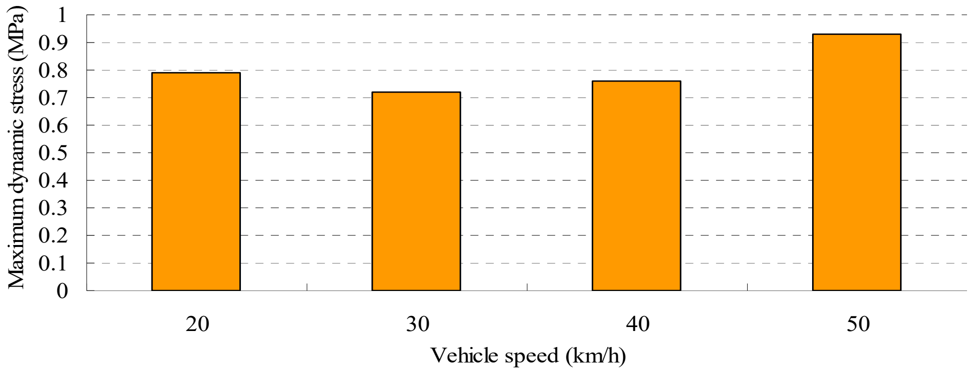

Figure 20. Maximum dynamic stresses measured in different vehicle speed cases.

6. Conclusions

The main findings of the present study concerning the effects of vehicle speed on the vehicle-induced dynamic behaviors of a concrete bridge with smooth and rough road surfaces are summarized below:

(1) It was observed via an on-location inspection in Ref. [4] that a concrete bridge supporting vehicles running at lower speeds suffers from more severe apparent damages compared with one supporting vehicles of higher speeds. However, with a smooth road surface (as assumed by the numerical simulations presented in Ref. [4]), the vehicle-induced structural response of a bridge was found to be greater for a high-vehicle-speed case than for a low-vehicle-speed case in this article. The present numerical simulations suggest that with a sufficient increase in road surface roughness, the resonant responses are significantly amplified for the low-vehicle-speed cases, and the vehicle-induced tensile stresses are therefore calculated to be close to the tensile strength of the concrete material for both the low-vehicle-speed case and the high-vehicle-speed case. Actual bridges are usually associated with high degrees of road surface roughness. Therefore, a bridge supporting vehicles of lower speeds should suffer from more severe damages, as the vehicle load holding duration is longer for the low-vehicle-speed case than for the high-vehicle-speed case. The practical implication of the present findings on concrete bridge maintenance and monitoring is that for bridges with a smooth road surface (newly built bridges), maintenance and monitoring should focus on supporting high-speed vehicles, while for bridges with sufficiently rough road surfaces (bridges in operation for years), maintenance and monitoring should focus on supporting low-speed vehicles.

(2) The field experiments undertaken by the present study further reveal the mechanism behind the observed phenomenon. It was found that merely considering the effects of road surface roughness, the frequency of vehicle excitation for a bridge with sufficient

road surface roughness should markedly decrease with the decrease in vehicle speed and becomes closer to the low-order natural frequencies of the bridge. Therefore, the resonant responses ought to be more significantly amplified for the lower-vehicle-speed case after the increase in road surface roughness.

(3) The existing literature separately considers the effects of road surface roughness and vehicle speed on vehicle–bridge coupling dynamics. However, no study has well revealed significant interactions between vehicle speed and road surface roughness in the context of vehicle–bridge coupling dynamics. This scientific gap is well filled in this article. Since only nine cases were considered for the present numerical simulations assuming a 30-ton vehicle running through Renyihe Bridge at three vehicle speeds (20 km/h, 50 km/h, and 90 km/h) with three road surface roughness levels (smooth, slightly rough, and severely rough), mathematical models accounting for the coupled road surface roughness and vehicle speed effects can hardly be established at present due to sample scarcity. However, after more cases have been studied on Renyihe Bridge or other bridges, we can formulate useful empirical formulae to quantitatively guide concrete bridge maintenance and monitoring in the future.

Although the present study indicates that the resonant responses are supposed to be more significantly amplified for the lower-vehicle-speed case after the increase in road surface roughness, it should be noted that for the rough road surface case, although the nature of vehicle excitation is influenced by the effects of road surface roughness when the vehicle speed is decreased, this influence is sometimes not sufficient to bring about the reduction in frequency of the vehicle's excitation, as the automobile engine frequency is markedly increased.

Finally, it should be admitted that although the present work contributes to the state of scientific knowledge, it is based on a single engineering case: Renyihe Bridge. In the future, more works are required to validate the results presently obtained using other examples of bridge types and vehicle excitations. In addition, other factors such as weather conditions, traffic volume, and construction quality can also impact bridge health and interact with vehicle speed and road surface roughness. Related research in the future can help pave a new path toward developing an inclusive math model for examining bridge health.

Author Contributions: Conceptualization, X.-X.C.; methodology, X.-X.C., Y.L. and J.-R.Q.; software, X.-X.C.; validation, L.D., M.-D.C., Z.-W.Z. and X.-X.C.; formal analysis, X.-X.C., Y.L. and J.-R.Q.; investigation, X.-X.C., Y.L. and J.-R.Q.; resources, X.-X.C.; data curation, X.-X.C., Y.L. and J.-R.Q.; writing—original draft preparation, L.D.; writing—review and editing, X.-X.C.; visualization, L.D.; supervision, X.-X.C.; project administration, X.-X.C.; funding acquisition, X.-X.C. All authors have read and agreed to the published version of the manuscript.

Funding: This research and the APC were funded by the Key Science and Technology Project of Jiangxi Provincial Department of Transportation (grant number 2019Z0002) and the Jiangxi Natural Science Foundation (grant number 20202BABL214043).

Data Availability Statement: The data presented in this study are available upon request from the corresponding authors.

Conflicts of Interest: The authors declare that there are no conflict of interest regarding the publication of this article.

References

1. Dong, Y.; Zhang, W.; Shamsabadi, A.; Shi, L.; Taciroglu, E. A Vehicle–Bridge Interaction Element: Implementation in ABAQUS and Verification. *Appl. Sci.* **2023**, *13*, 8812. [CrossRef]
2. Chen, D.; Zhu, C.; Shi, X.; Song, J. Influence of Random Vehicle–Bridge Coupling Vibration on the Anti-Disturbance Performance of Concrete Materials. *Appl. Sci.* **2023**, *13*, 7584. [CrossRef]
3. Rossigali, C.E.; Pfeil, M.S.; Sagrilo, L.V.; de Oliveira, H.M. Load Models Representative of Brazilian Actual Traffic in Girder-Type Short-Span Highway Bridges. *Appl. Sci.* **2023**, *13*, 1032. [CrossRef]
4. Cai, Y.; Nie, L.; Cheng, X. Research on the distribution rules of cracks on reinforced concrete continuous girder bridge deck of in-service expressway and the formation mechanisms. *Highway* **2020**, *36*, 136–142. (In Chinese)

5. Li, Z.; Au, F.T.K. Damage detection of bridges using response of vehicle considering road surface roughness. *Int. J. Struct. Stab. Dyn.* **2015**, *15*, 1450057. [CrossRef]
6. Yang, Y.B.; Li, Y.C.; Chang, K.C. Using two connected vehicles to measure the frequencies of bridges with rough surface: A theoretical study. *Acta Mech.* **2012**, *223*, 1851–1861. [CrossRef]
7. Yang, Y.B.; Li, Y.C.; Chang, K.C. Effect of road surface roughness on the response of a moving vehicle for identification of bridge frequencies. *Interact. Multiscale Mech.* **2012**, *5*, 347–368. [CrossRef]
8. Deng, L.; Cai, C.S. Identification of parameters of vehicles moving on bridges. *Eng. Struct.* **2009**, *31*, 2474–2485. [CrossRef]
9. Zhu, X.Q.; Law, S.S. Moving load identification on multi-span continuous bridges with elastic bearings. *Mech. Syst. Signal Process.* **2006**, *20*, 1759–1782. [CrossRef]
10. Kiani, K.; Nikkhoo, A.; Mehri, B. Assessing dynamic response of multispan viscoelastic thin beams under a moving mass via generalized moving least square method. *Acta Mech. Sin.* **2010**, *26*, 721–733. [CrossRef]
11. Johansson, C.; Pacoste, C.; Karoumi, R. Closed-form solution for the mode superposition analysis of the vibration in multi-span beam bridges caused by concentrated moving loads. *Comput. Struct.* **2013**, *119*, 85–94. [CrossRef]
12. Szyłko-Bigus, O.; Śniady, P.; Zakęś, F. Application of Volterra integral equations in the dynamics of a multi-span Rayleigh beam subjected to a moving load. *Mech. Syst. Signal Process.* **2019**, *121*, 777–790. [CrossRef]
13. Kiani, K.; Roshan, M. Nonlocal dynamic response of double-nanotube-systems for delivery of lagged-inertial-nanoparticles. *Int. J. Mech. Sci.* **2019**, *152*, 576–595. [CrossRef]
14. Yu, G.; Kiani, K.; Roshan, M. Dynamic analysis of multiple-nanobeam-systems acted upon by multiple moving nanoparticles accounting for nonlocality, lag, and lateral inertia. *Appl. Math. Model.* **2022**, *108*, 326–354. [CrossRef]
15. Abdelrahman, A.A.; Esen, I.; Ozarpa, C.; Shaltout, R.; Eltaher, M.A.; Assie, A.E. Dynamics of perforated higher order nanobeams subject to moving load using the nonlocal strain gradient theory. *Smart Struct. Syst.* **2021**, *28*, 515–533.
16. Hosseini, S.A.; Rahmani, O.; Bayat, S. Thermal effect on forced vibration analysis of FG nanobeam subjected to moving load by Laplace transform method. *Mech. Based Des. Struct. Mach.* **2023**, *51*, 3803–3822. [CrossRef]
17. Fan, J.H.; Xiao, Z.H.; Cheng, X.X. Numerical Simulations of Modal Tests on Yingzhou Bridge Using a Passing Vehicle as the Excitation. *Exp. Tech.* **2022**, *46*, 529–541. [CrossRef]
18. Huang, X.Y. Dynamic Response Research of Continuous Curved Concrete Bridges Under Moving Vehicles. Ph.D. Thesis, Harbin Institute of Technology, Harbin, China, 2008. (In Chinese)
19. Cheng, X.X.; Liao, Y.C. Structural Safety Assessment Oriented Modal Experiments on Renyihe Bridge Using Vehicle Excitations. *Structures* **2023**, *accepted*. [CrossRef]
20. Shanxi Provincial Transportation Construction Engineering Quality Testing Center. *Load Test and Inspection Report of Renyihe Bridge*; Report GL-2021-0019; Shanxi Provincial Transportation Construction Engineering Quality Testing Center: Taiyuan, China, 2021.